Optical isotopic shifts and hyperfine splittings for Yb

D. L. Clark,* M. E. Cage,† D. A. Lewis,‡ and G. W. Greenlees
Department of Physics, University of Minnesota, Minneapolis, Minnesota 55455
(Received 15 May 1978)

A cw tunable dye laser and atomic-beam techniques were used to determine the splittings and separations of the natural Yb isotopes for the 5556.5-Å, $^3P_1$-$^1S_0$ transition. The resonant scattering was recorded with an instrumental resolution of 7 MHz full width at half-maximum, giving peak separations accurate to ± 0.5 MHz. The hyperfine splittings were analyzed to yield values of $-0.382(19)\%$ for the hyperfine anomaly and 10.9 GHz/fm^2 for the field-shift constant; these agree with published values. The optical isotope shifts obtained, along with published electronic and muonic x-ray shifts, were analyzed to yield $\delta\langle r^2\rangle$ values and a specific mass shift in the range 200–300 MHz. This latter is considerably greater than is normally used for $6s^2$-$6s6p$ transitions. The model dependence of the isotopic-shift analysis was examined, and the hyperfine anomaly was compared with calculations based on Nilsson wave functions.

I. INTRODUCTION

The study of isotope shifts and hyperfine structure of optical transitions in atomic spectra has been an important source of information on electric and magnetic moments from the very beginnings of nuclear physics. Isotopic shifts yield detailed information about the changes in the radial moments of the nuclear charge distribution between isotopes, and the hyperfine structure allows accurate measurements of electric and magnetic moments of the nucleus. Very precise measurements are even capable of yielding information about the changes in the nuclear magnetization distribution between isotopes. Recent developments in dye-laser technology promise a significant increase in the quantity and quality of such data.

The high resolution obtained by the use of tunable cw dye lasers in atomic and molecular spectroscopy is well known[1] and makes possible measurements for a large number of elements, limited in resolution only by the natural linewidth of the optical transition. Furthermore, such measurements can be made with atomic beam fluxes as low as 10 atoms/sec.[2] Such capabilities will have important consequences in the study of electric and magnetic moments of short-lived nuclei which has already produced interesting results for Hg, Na, Cs, and Ba.[3]

The present paper reports measurements of the isotopic shifts and the hyperfine splittings of all the naturally occurring Yb isotopes, for the 5556.5-Å transition, using an atomic beam and a cw tunable dye laser. The separations of all the components of the fluorescent spectrum are determined to ± 0.5 MHz, without the use of isotopically enriched samples. An analysis of the hyperfine components of the odd isotopes yields values for the hyperfine anomaly (HFA) and the field-shift constant. The isotopic shifts, together with published electronic and muonic x-ray data, are analyzed to obtain the size differences between isotopes. This analysis suggests that the specific mass shift for the $6s^2$-$6s6p$, 5556-Å transition of Yb is much larger than has been used previously. The HFA results are compared with nuclear calculations based on Nilsson wave functions.

II. EXPERIMENTAL APPARATUS

A block schematic of the experimental arrangement is shown in Fig. 1. The 5145-Å single line output of the argon ion laser (Spectra Physics 164-03) pumps the cw tunable dye laser (Spectra Physics 580-01). The output from the dye laser, tunable via piezoelectric crystals in the cavity, orthogonally intersects a collimated atomic beam (A) and the scattered light is detected by a photomultiplier, operating in the single photon counting mode, as a function of the dye-laser frequency. The rate of detection of scattered photons is normalized to the dye-laser output via the monitoring photodiode PD1, and fed to the y axis of an x-y recorder. This latter is swept in the x direction by the same ramp voltage which sweeps the dye-laser frequency. The instrumental resolution obtained is 7 MHz (full width at half maximum, FWHM); the largest contribution to this width comes from the dye laser.

In order to obtain accurate measurements of peak separations, a set of frequency markers are recorded simultaneously with the optical spectra. These markers are generated using the stabilized He-Ne laser (Spectra Physics 119) and the confocal Fabry-Perot etalon (Tropel 216V). The center of the He-Ne laser oscillation is servo-locked to the center of the Lamb dip (via PD4) and the etalon cavity length is, in turn, servo-locked to a trans-

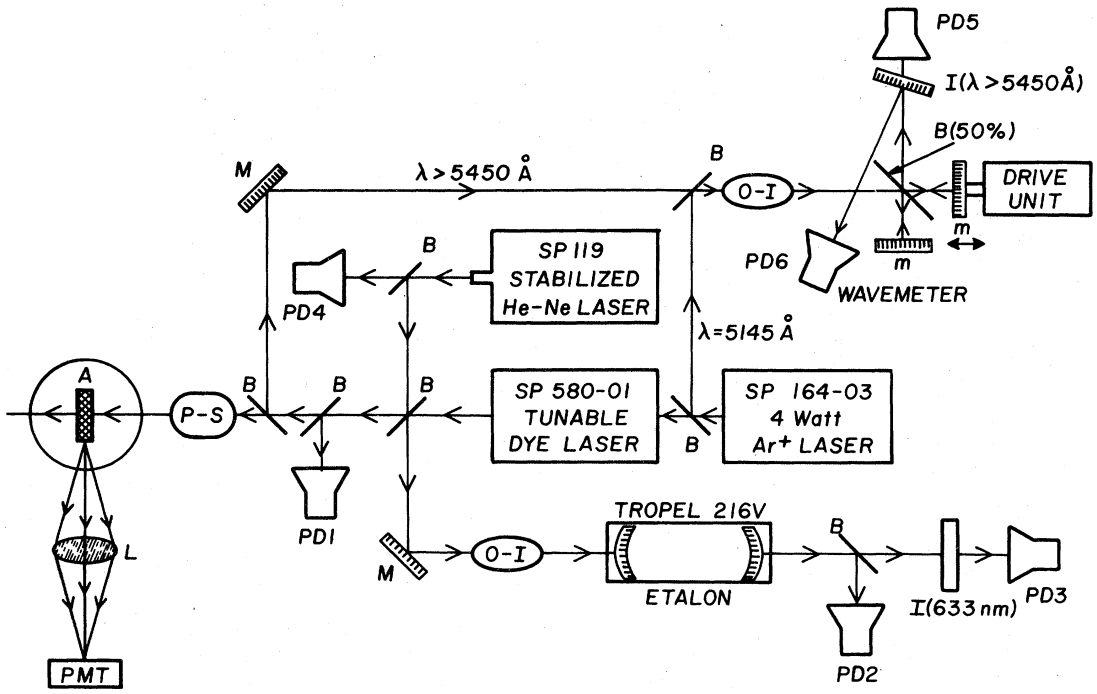

FIG. 1. Block diagram of system. A, atomic beam; B, beam splitter; M,m, mirror; PD, photodiode; I, filter; OI, optical isolator; PS, polarization selector; PMT, photomultiplier tube.

mission peak of the He-Ne output (via PD3). The cavity length is thus stabilized to 0.1 MHz. A fraction of the dye-laser output is also fed through the etalon, giving transmission peaks every free spectral range (300.35 ± 0.05 MHz), as the dye laser is swept. These peaks are detected in PD2 and used to generate markers spaced at 300.35-MHz intervals. Facilities are incorporated which enable the order of the He-Ne transmission peak, to which the etalon is locked, to be changed successively by one order. This arrangement has been described previously[4] and produces markers spaced at intervals of $300.35(\lambda_{\text{He-Ne}}/\lambda_{\text{dye}} - 1)$ MHz. This corresponds to a 41.7-MHz spacing in the case of the 5556-Å line of Yb. The etalon length is stabilized at 6328 Å, whereas the transmission peaks of the dye-laser light are at 5556 Å. The difference in the index of refraction at these wavelengths results in movement of the marker positions with pressure changes in the etalon. This effect was eliminated by operating the confocal etalon in an evacuated chamber.

To facilitate the location of optical resonances, a wavemeter is used. This comprises a Michelson interferometer which compares the number of fringes from collinear beams of dye-laser light and the 5145.38-Å line of the argon ion laser, as the path difference of one of the interferometer arms is varied. The path change is effected by mounting one of the mirrors on a Mössbauer drive unit which is driven back and forth continuously for a distance of about 1.5 cm with a period of about 1 sec. The two sets of fringes are counted separately over the central portions of the sweeps. Approximately 3×10^4 fringes per sweep are counted giving an accuracy of about 0.2 Å in the determination of the dye-laser wavelength for a single sweep of the mirror. This accuracy can be improved by suitably averaging sweeps.

A diagram of the atomic beam scattering chamber is shown in Fig. 2. The atomic beam is defined by two slits, one at the top of the electrically heated molybdenum oven and the other just below the chamber center. The slits are each 0.050 in. wide and are separated by about 30 in. Light collection consists of a spherical concave mirror and a pair of two-element condenser lenses which focus the light through a slit and onto a 56 AVP photomultiplier tube (PMT). Approximately 14% of the fluorescent light reaches the PMT.

The laser beam is carefully baffled and enters the chamber normal to Fig. 2, where it intersects the atomic beam at the center and subsequently leaves the chamber through a window. The chamber was evacuated by an ion pump, to pressures around 10^{-8}–10^{-9} Torr. The Helmholtz coils enabled uniform magnetic fields up to 350 G to be applied to the center of the chamber.

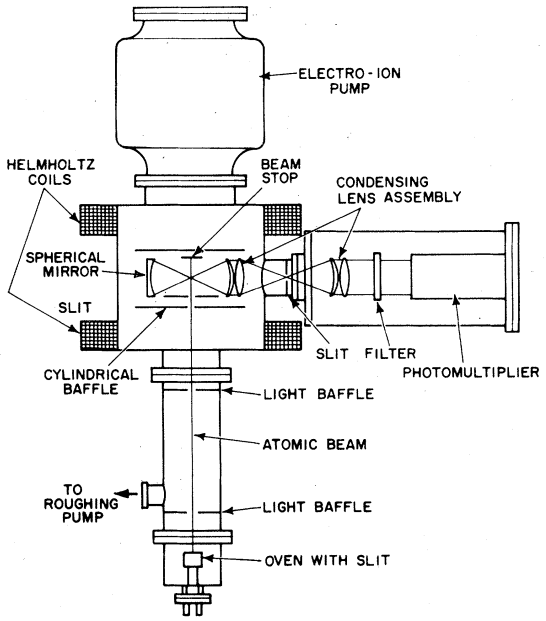

FIG. 2. Scattering chamber. The laser beam enters the chamber normal to the figure.

In order to eliminate significant differential Doppler shifts between isotopes, due to different average thermal velocities and a nonzero average component of velocity parallel to the laser beam, the later was retroreflected through the atomic beam and the observed linewidth was minimized.

III. EXPERIMENTAL DATA

A composite of two wide sweeps of the 5556.5-Å transition of Yb is shown in Fig. 3(a). The observed transitions are labeled to indicate the isotope responsible and, for the odd-A isotopes, the F quantum numbers of the hyperfine component for the ground and excited state. The 300-MHz frequency markers are also shown. Figure 3(b) shows a narrow scan of the type used to generate data. The resolution of the laser system is seen to be ~ 7-MHz FWHM and narrow markers, generated by hopping the mode of the He-Ne laser-etalon system, are shown. Since natural abundance samples were used, the line due to ^{168}Yb, is very weak. Figure 3(c) shows this line together with the nearby lines due to the $F_{ex}=\frac{3}{2}$ components of ^{171}Yb and ^{173}Yb.

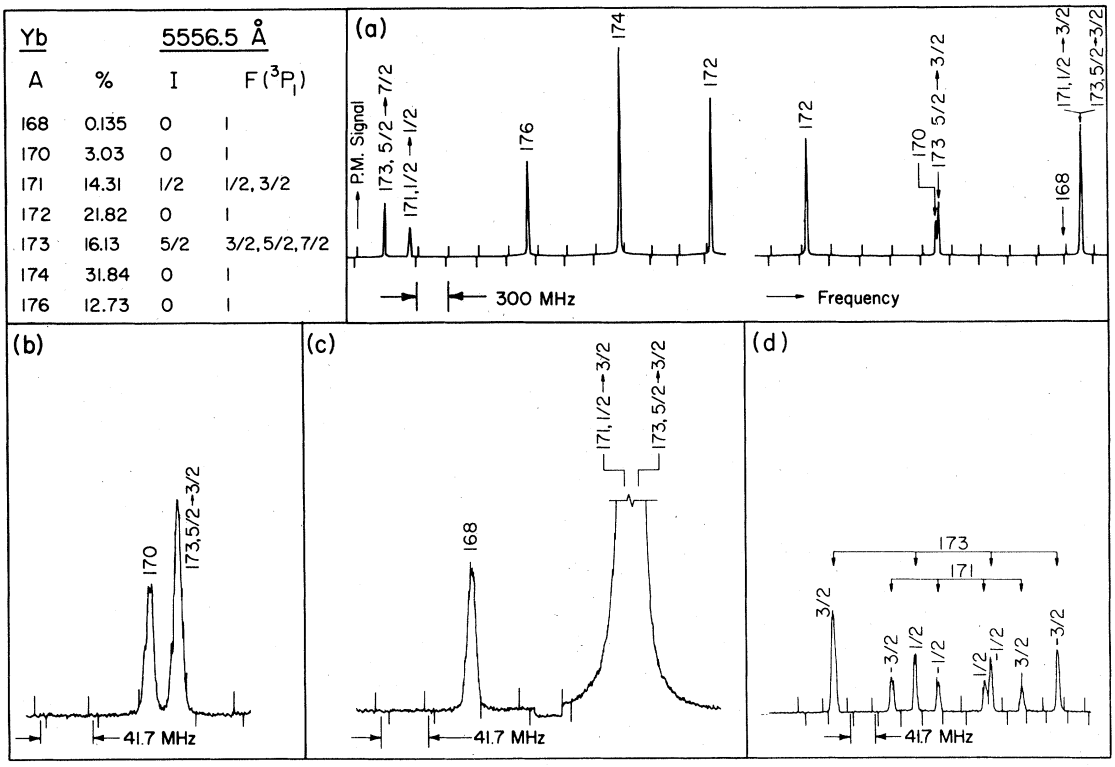

FIG. 3. Fluorescent spectra for the 5556.6-Å transition in YbI. (a) Wide scan showing 300.35-MHz markers. Lines are labeled according to isotope and F quantum numbers (odd isotopes). (b) Narrow sweep of type used to accumulate data with 41.7-MHz markers. (c) Narrow sweep showing line due to ^{168}Yb (0.14% abundant). For part of the sweep between the two peaks, the laser beam was blocked from entering the chamber. (d) Zeeman pattern used to separate lines due to ^{171}Yb($F=\frac{1}{2}\rightarrow\frac{3}{2}$ and ^{173}Yb($F=\frac{5}{2}\rightarrow\frac{3}{2}$) transitions. Individual lines labeled by M_F values of the excited state.

The lines due to the $F_{ex}=\frac{3}{2}$ components of ^{171}Yb and ^{173}Yb were unresolved and analysis of the unresolved linewidth indicated their separation was less than 2 MHz. In order to determine more precisely the line positions, a 102-G magnetic field was applied in a direction perpendicular to the plane of the laser beam and photomultiplier, and parallel to the polarization of the laser beam. The Zeeman splitting is shown in Fig. 3(d). Due to the different gyromagnetic ratios for the isotopes ^{171}Yb and ^{173}Yb, the splitting is unequal and the components of the two isotopes are separated. Corrections as large as 17 MHz were made to some of the components to compensate for off-diagonal matrix elements in the Zeeman interaction and zero-field line positions were computed. In order to avoid blended components, only the $M_F=\pm\frac{3}{2}$ components were used.

When analyzing data sweeps of the type shown in Figs. 3(b), 3(c) or 3(d), the line positions were determined by fitting a quadratic to the measured positions of five calibration markers and interpolating the positions of the data peaks. Nine to twelve sweeps over each line were recorded and analyzed. Standard deviations of the measurements were between 0.38 and 0.87 MHz, which implies a variance in the average of ≤ 0.3 MHz. Systematic errors in the data have been examined by a series of measurements in Sm, Dy, and Er, for which the measured splitting is entirely due to hyperfine splitting in the ground state. The ground-state hyperfine splitting has been accurately measured using radio-frequency techniques.[5] Thirty such cases were measured and indicated that the systematic error is about 0.5 MHz. Since this is larger than the variance in the average, we assign an error of ± 0.5 MHz to our measurements. The resulting line positions are listed in Table I.

IV. ANALYSIS OF HYPERFINE SPLITTINGS

A. Formalism

The hyperfine splitting of atomic energy levels is due to the interaction of the electrons with the nuclear currents and the nonspherical components of the nuclear charge distribution. Analysis of this splitting yields information on nuclear magnetic dipole moments and electric quadrupole moments and, for extremely accurate measurements, may yield information about even higher-order moments. In addition, since the electrons have a nonzero density within nuclear dimensions, there are small effects due to the spatial distribution of the nuclear charge and currents. The major effect of the spatial distribution of nuclear charge is the isotope shift, although, in principle, there is a small effect on the hyperfine splitting due to higher electric moments. An observable effect of the spatial distribution of nuclear currents is a small change in the magnetic dipole splitting. When hyperfine splittings for two odd isotopes, are available, these changes can be detected assuming the nuclear magnetic moments are known. Such effects are expressed as a hyperfine anomaly parameter.

Neglecting the small effects due to electron density within nuclear dimensions, the perturbation Hamiltonian due the interaction of atomic electrons

TABLE I. Experimental data on isotope shifts and hyperfine splittings of the 5556.5-Å transition of YbI. Hyperfine components labeled with an asterisk were determined from the Zeeman splittings as described in the text. Previous measurements due to Ross [J. Opt. Soc. 53, 299 (1963); 66 585 (1976)] and Chaiko [Opt. Spectrosc. 20 424 (1970)] are given in columns 3 and 4.

Spectral component	Position relative to ^{176}Yb (MHz) Present work	Ross	Chaiko
$173(\frac{5}{2}\rightarrow\frac{7}{2})$	−1431.73(50)	−1460 (6)	−1451(6)
$171(\frac{1}{2}\rightarrow\frac{1}{2})$	−1177.23(50)	−1187 (3)	−1184(6)
176	0	0	0
174	954.76(50)	947 (2)	947(2)
172	1955.04(50)	1940 (9)	1940(9)
170	3241.51(50)	3229(18)	3232(6)
$173(\frac{5}{2}\rightarrow\frac{5}{2})$	3266.49(50)	3247 (9)	3253(6)
168	4610.14(50)	4581(15)	...
$171(\frac{1}{2}\rightarrow\frac{3}{2})$	4759.83(50)*	4761 (9)	4761(9)
$173(\frac{5}{2}\rightarrow\frac{3}{2})$	4760.42(50)*	4749(12)	4700(6)

with the nuclear charge and current distribution can be written in the form

$$H_{\rm hfs}=\sum_k T_E^{(k)}T_N^{(k)}, \tag{1}$$

where for even k the operators are given by

$$T_E^{(k)}=\sum_{j=1}^{z}(-e)\left(\frac{1}{r_{ej}^{k+1}}\right)C^{(k)}(\hat{r}_{ej}),$$
$$T_N^{(k)}=\sum_{j=1}^{A} eg_{lj}r_{nj}^{k}C^{(k)}(\hat{r}_{nj}); \tag{2}$$

and for odd k

$$T_E^{(k)}=\sum_{j=1}^{z} ie\sqrt{2}\left(\frac{1}{r_{ej}^{k+1}}\right)(\bar{\alpha}C_j^{(k)})^{(k)},$$
$$T_N^{(k)}=\mu_N\sum_{j=1}^{A}[k(2k-1)]^{1/2}r_n^{k-1}$$
$$\times\left(\frac{2g_{lj}}{k+1}(C_j^{(k-1)}l_{nj})^{(k)}+g_{sj}(C_j^{(k-1)}s_{nj})^{(k)}\right). \tag{3}$$

The notation is standard and conforms to Ref. 6. Matrix elements of the hyperfine interaction Hamiltonian can be written

$$\langle\lambda JIFM_F|H_{\rm hfs}|\lambda'J'I'F'M_F'\rangle$$
$$=\delta_{FF'}\delta_{M_FM_F'}(-1)^{I+J'+F}\sum_k\begin{Bmatrix}J&I&F\\I'&J'&K\end{Bmatrix}\langle\gamma J||T_E^{(k)}||\gamma'J'\rangle$$
$$\times\langle\beta I||T_N^{(k)}||\beta'I'\rangle. \tag{4}$$

The hyperfine Hamiltonian is not diagonal in J or I, but we consider first-order perturbations and take $\gamma=\gamma'$, $J=J'$, $\beta=\beta'$, and $I=I'$. The latter two equalities are very good approximations since the interaction energies of the electrons are small compared with nuclear energy levels. The assumptions that $\gamma=\gamma'$ and $J=J'$ are less valid and will require small corrections. First-order perturbation energies are given by

$$\Delta E_F^{(1)}=(-1)^{I+J+F}\sum_k\begin{Bmatrix}JIF\\IJk\end{Bmatrix}\langle\gamma J||T_E^{(k)}||\gamma J\rangle$$
$$\times\langle\beta I||T_N^{(k)}||\beta I\rangle$$
$$\equiv(-1)^{I+J+F}\sum_k\left[\begin{Bmatrix}JIF\\IJk\end{Bmatrix}\Big/\begin{pmatrix}JKJ\\JOJ\end{pmatrix}\begin{pmatrix}IkI\\IOI\end{pmatrix}\right]A_k. \tag{5}$$

The second equation defines the parameter A_k. It is easy to show that the "center of gravity" of the hyperfine splitting is unchanged by the $k>0$ components of the first-order perturbation energy, so that

$$\sum_F(2F+1)\Delta E_F^{(1)}=0. \tag{6}$$

This allows the centroid to be determined and the isotope shift to be extracted. The isotope shift may require some correction due to second-order effects.

The orthogonality relationships of the 6-j symbols make it possible to invert the equation for $\Delta E_F^{(1)}$ to obtain an equation for A_k:

$$A_k=\begin{pmatrix}JkJ\\JOJ\end{pmatrix}\begin{pmatrix}IkI\\IOI\end{pmatrix}(2k+1)$$
$$\times\sum_F(-1)^{I+J+F}(2F+1)\begin{Bmatrix}JIF\\IJK\end{Bmatrix}\Delta E_F(1). \tag{7}$$

The usual dipole and quadrupole coupling constants A and B are defined[7] by

$$A=(1/IJ)A_1\equiv(\mu_I/IJ)\langle\gamma JJ|T_E^{(1)}|\gamma JJ\rangle,$$
$$B=4A_2\equiv 2eQ\langle\gamma JJ|T_E^{(2)}|\gamma JJ\rangle, \tag{8}$$

where μ_I is the nuclear magnetic moment and Q is the nuclear electric quadrupole moment.

Equation (8) implies the ratio of dipole coupling constants, A, for two isotopes will be equal to the ratio of the magnetic g factors ($g_I\equiv\mu_I/I$). Deviations from this rule arise from the finite size of the distribution of nuclear magnetism and are parametrized by the hyperfine anomaly (HFA) Δ_{12}, where

$$\frac{A(1)}{A(2)}=\frac{g_I(1)[1-\epsilon(1)]}{g_I(2)[1-\epsilon(2)]}=\frac{g_I(1)}{g_I(2)}(1-\Delta_{12}). \tag{9}$$

The experimentally observable quantity is Δ_{12}.

If we describe the nuclear ground state using Nilsson wave functions of the form[8]

$$|\psi\rangle=\sum_j C_j|Nlj\Omega\rangle, \tag{10}$$

it is possible to show[9] that ϵ is given by the expression

$$\epsilon=\frac{1}{\mu_I}\left(\frac{I}{I+1}\right)\Bigg\{\sum_{jj'}(-1)^{j-I}C_jC_{j'}\left[\begin{pmatrix} j & 1 & j' \\ I & 0 & I\end{pmatrix}-(-1)^{j'+1/2}\sqrt{2}\begin{pmatrix} j & 1 & j' \\ I & 1 & I\end{pmatrix}\delta_{k,1/2}\right]$$

$$\times\Big[\sum_k g_e(b_L)_{2k}\langle j\,||L_z(r^2/R_0^2)^k||j'\rangle+g_s(b_s)_{2k}\langle j\,||S_z(r^2/R_0^2)^k||j'\rangle$$

$$+g_s(b_p)_{2k}\langle j\,||(\tfrac{5}{2})^{1/2}(C^{(2)}\mathrm{S})^{(1)}(r^2/R_0^2)^k||j'\rangle\Big]+g_R(1+a\delta_{k,1/2})\sum_k(b_L)_{2k}\nu_k\Bigg\}. \quad (11)$$

μ_I is the nuclear magnetic moment in nuclear magnetons. $(b_L)_{2k}$, $(b_s)_{2k}$, and $(b_p)_{2k}$ are atomic parameters defined by Stroke *et al.*[10] and can be obtained from their tables for $s_{1/2}$ and $p_{1/2}$ electron configurations. The parameter ν_k is a variable introduced by Reiner[11] to parametrize the radial distribution of the nuclear current, due to the collective rotation. He has shown, for example, that $\nu_2=1$ for incompressible flow and $\nu_2=\frac{5}{7}$ for rigid-body rotation. a is the standard "decoupling parameter."[8]

The reduced matrix elements in Eq. (11) can be written as a product:

$$\langle Nlj\,||A_{\mathrm{op}}(r^2/R_0^2)^k||Nl'j'\rangle$$

$$=\langle Nlj\,||A_{\mathrm{op}}||Nl'j'\rangle\langle Nl\,|r^{2k}|Nl'\rangle R_0^{2k}. \quad (12)$$

The radial integrals can be parametrized by defining[11]

$$\sigma\equiv(1/R_0^2)\langle Nl\,|r^2\,|Nl\rangle, \quad (13)$$

so that we can write

$$\langle Nl\,|(r^2/R_0^2)^k|Nl'\rangle=\sigma^k\frac{\langle Nl\,|r^{2k}|Nl'\rangle}{\langle Nl\,|r^2|Nl\rangle^k}$$

$$\equiv\sigma^k R(Nl,Nl',k), \quad (14)$$

where R can be computed using harmonic-oscillator wave functions.[12]

When computing Δ_{12} using Eq. (9), it is first necessary to correct the magnetic dipole coupling constants $A(i)$ for second-order matrix elements. In addition, computation of $\epsilon(i)$ involves only the effect of $s_{1/2}$ or $p_{1/2}$ electrons (since only they have significant density within nuclear dimensions) whereas the $A(i)$'s involves the coupling of all electrons to the nuclear magnetic moment. Consequently, in order to analyze the HFA it is necessary to analyze the hyperfine splitting to extract atomic parameters which will allow second-order corrections to be computed and also to determine the contribution of the various electron types within the electron configuration to the magnetic dipole coupling constant.

Using the effective operator formalism of Sandars and Beck,[13] the electron operators within a l^N configuration can be written in the form

$$T_E^{(1)}=\mu_0\sum_i\frac{4}{3}\left\langle\frac{\delta(r_i)}{r_i^2}\right\rangle_{10}s_i+2\left\langle\frac{1}{r_i^3}\right\rangle_{01}l_i$$

$$+2\sqrt{10}\left\langle\frac{1}{r_i^3}\right\rangle_{12}(s_iC^{(2)})^{(1)}$$

$$T_E^{(2)}=e\sum_i\left\langle\frac{1}{r_i^3}\right\rangle_{11}(s_il_i)^{(2)}+\left\langle\frac{1}{r_i^3}\right\rangle_{13}$$

$$\times[s_i(C_i^{(4)}l_i)^{(3)}]^{(2)}-\left\langle\frac{1}{r_i^3}\right\rangle_{02}C_i^{(2)}, \quad (15)$$

where μ_0 is the Bohr magneton and the quantities $\langle\ \rangle_{pq}$ are relativistic radial integrals.[13] Within the central field approximation, a configuration of the type [core] 6s6p requires four radial integrals for the magnetic dipole coupling constant (one for the s electron, three for the p electron) and two for the quadrupole coupling constant (both for the p electron). Measurement of the hyperfine splitting of four or more levels of the configuration allows the radial integrals to be treated as unknown parameters and fit to the experimental data. It is then possible to use the radial integrals to compute both diagonal and off-diagonal matrix elements for levels of that configuration.

If measurements are available for fewer levels than are required to determine the radial integrals, the number of unknown radial integrals can be reduced using an approximate procedure based on the relativistic correction factors (RCF) of Kopferman.[14] This approximation yields for the magnetic dipole case

$$\left\langle \frac{\delta(r)}{r^2} \right\rangle_{10}(nl) = \frac{2l(l+1)}{(2l+1)^2}[(l+1)F(l,j=l+\tfrac{1}{2}) - G(l) - lF(l,j=l-\tfrac{1}{2})]\langle 1/r^3\rangle_M(nl),$$

$$\left\langle \frac{1}{r^3} \right\rangle_{01}(nl) = \frac{1}{(2l+1)^2}[2l(l+1)F(l,j=l+\tfrac{1}{2}) + G(l) + 2l(l+1)F(l,j=l-\tfrac{1}{2})] \times \langle 1/r^3\rangle_M(nl), \tag{16}$$

$$\left\langle \frac{1}{r^3} \right\rangle_{12}(nl) = \frac{1}{3(2l+1)^2}[4l(l+1)(2l-1)F(l,j=l+\tfrac{1}{2}) + (2l-1)(2l+3)G(l) - 4l(2l+3)(l+1)F(l,j-\tfrac{1}{2})] \times \langle 1/r^3\rangle_M(nl);$$

and for the electric quadrupole

$$\left\langle \frac{1}{r^3} \right\rangle_{02}(nl) = \frac{1}{(2l+1)^2}[(2l-1)(l+2)R(l,j=l+\tfrac{1}{2}) + 6S(l) + (l-1)(2l+3)R(l,j=l-\tfrac{1}{2})] \times \langle 1/r^3\rangle_Q(nl),$$

$$\left\langle \frac{1}{r^3} \right\rangle_{11}(nl) = \frac{2\sqrt{6}}{5(2l+1)^2}[(l+2)R(l,j=l+\tfrac{1}{2}) + 3S(l) + (l-1)R(l,j=l-\tfrac{1}{2})] \times \langle 1/r^3\rangle_Q(nl),$$

$$\left\langle \frac{1}{r^3} \right\rangle_{13}(nl) = \frac{4\sqrt{21}}{5(2l+1)^2}[2(l-1)R(l,j=l+\tfrac{1}{2}) + 4S(l) - (2l+3)R(l,j=l-\tfrac{1}{2})] \times \langle 1/r^3\rangle_Q(nl). \tag{17}$$

Similar equations have been used by Childs and Goodman.[15]

These relationships allow the number of radial integrals in the expressions for the magnetic dipole and electric quadrupole coupling constants to be reduced to one for each of the nonequivalent electron types in the configuration.

Second-order perturbation energies are given by[6]

$$\Delta E^{(2)} = \sum_r (-1)^{I+J+F}\begin{Bmatrix} J & I & F \\ I & J & r \end{Bmatrix} \sum_{\substack{J'I' \\ kq}} (-1)^{2I'+2J'+k+q+r} \frac{2r+1}{(E_J - E'_J)+(E_I - E_{I'})} \begin{Bmatrix} k & q & r \\ I & I & I' \end{Bmatrix} \begin{Bmatrix} k & q & r \\ J & J & J' \end{Bmatrix} \times \langle I||T_N^{(k)}||I'\rangle\langle I'||T_N^{(q)}||I\rangle\langle J||T_E^{(k)}||J'\rangle\langle J'||T_E^{(q)}||J\rangle. \tag{18}$$

We will assume $I = I'$. This assumption is justified by the large energy denominator that would be introduced by $I' \neq I$ and this assumption has the effect of limiting the tensor operators to cases which have nonzero diagonal nuclear matrix elements. Since the diagonal matrix elements of the nuclear operators are large only for $M1$ and $E2$ operators, we need to consider $M1 - M1$, $M1 - E2$, and $E2 - E2$ combinations. The nuclear matrix elements are easily evaluated from

$$(I||T_n^{(1)}||I) = \left(\frac{(I+1)(2I+1)}{I}\right)^{1/2}\mu_I,$$

$$(I||T_n^{(2)}||I) = \frac{I(2I-1)}{[(2I-1)(2I+1)(I+1)(2I+3)]^{1/2}}\frac{eQ}{2}. \tag{19}$$

The reduced matrix elements of the electron operators can be computed in terms of the relativistic radial integrals, which can be obtained with sufficient accuracy from an analysis the first-order hyperfine splitting.

The $r = 0$ term results in a uniform displacement of all the hyperfine components of a level given by

$$\Delta E^{(2)}(r=0) = \frac{1}{(2IJ)(2J+1)} \times \sum_{kJ'} (-1)^{2I+J+J'}\left(\frac{1}{E_J - E_{J'}}\right) \times |\langle I||T_N^{(k)}||I\rangle|^2 |\langle J||T_E^{(k)}||J'\rangle|^2. \tag{20}$$

This results in a small displacement of the center of gravity of the hyperfine splitting and will effect

the observed isotope shift obtained using Eq. (6).

The $r=1$ term results in a correction to the dipole coupling constant A given by

$$A^{(2)}=\frac{1}{IJ}\sum_{\substack{J'\\kq}}(-1)^{2I+2J'+k+q+1}\left(\frac{3}{E_J-E_{J'}}\right)\begin{Bmatrix}k & q & l\\ I & I & I\end{Bmatrix}\begin{Bmatrix}k & q & l\\ J & J & J'\end{Bmatrix}$$

$$\times\langle I||T_N^{(k)}||I\rangle\langle I||T_N^{(q)}||I\rangle$$

$$\times\langle J||T_E^{(k)}||J'\rangle\langle J'||T_E^{(q)}||J\rangle\,. \qquad (21)$$

B. Ytterbium

The line positions of the hyperfine components of ^{171}Yb and ^{173}Yb are listed in Table I, and have been used, with Eqs. (6), (7), and (8), to compute the center of gravity and the magnetic dipole and electric quadrupole coupling constants. The results are listed in Table II. Magnetic octupole constants were computed and found to be smaller than experimental error. The Yb $^1S_0$ ground state is built on the $4f^{14}6s^2$ configuration. The excited-state configuration for the 5556.5-Å line studied, is $4f^{14}6s6p$ and is almost a pure $^3P_1$ term.[16]

The magnetic dipole coupling constant for the states of the $6s6p$ configuration can be written in terms of four radial integrals. Using the RCF's this number can be reduced to one for the s electron, $\langle\delta(r)/r^2\rangle_{10}(s)$, and one for the p electron, $\langle 1/r^3\rangle_{\rm NR}(p)$. Using Eq. (17) we find

$$\langle\delta(r)/r^2\rangle_{10}(p)=-0.2512\langle 1/r^3\rangle_{\rm NR},$$

$$\langle 1/r^3\rangle_{01}(p)=1.3458\langle 1/r^3\rangle_{\rm NR},$$

$$\langle 1/r^3\rangle_{12}(p)=1.9173\langle 1/r^3\rangle_{\rm NR},$$

where $\langle 1/r^3\rangle_{\rm NR}$ is the nonrelativistic expectation value. Using these expressions, $a_0^3\mu_N\mu_0=47.705$ MHz (μ_N is the nuclear magneton, μ_0 is the Bohr magneton) and $\mu_I=0.6779930(33)\mu_N$,[17] along with the simple wave functions of Bauman and Wandel,[16] gives for ^{173}Yb

$$A(^3P_1)=-5.848\langle\delta(r)/r^2\rangle_{10}(s)$$
$$-46.058\langle 1/r^3\rangle_{\rm NR}(p),$$

$$A(^3P_2)=-4.308\langle\delta(r)/r^2\rangle_{10}(s)$$
$$-11.382\langle 1/r^3\rangle_{\rm NR}(p),$$

$$A(^1P_1)=1.526\langle\delta(r)/r^2\rangle_{10}(s)$$
$$-39.162\langle 1/r^3\rangle_{\rm NR}(p).$$

The radial integrals are in units of a_0^{-3} and the A's are in MHz.

The present work yields 1094.20(60) MHz for $A(^3P_1)$. Published values[18-21] for $A(^3P_2)$ and $A(^1P_1)$ are −737.7 and 58.72 MHz, respectively. The three measured values of A form an overdetermined set of equations, but as has been previously noted,[20,22] it is not possible to get a good simultaneous fit to the singlet and triplet states. This is thought to be due to admixtures of the configuration $f^{-1}d$ in the $^1P_1$ state. In view of this difficulty, the radial parameters are derived using only the triplet states. This yields

$$a_0^3\langle\delta(r)/r^2\rangle_{10}(s)=163.2,$$

$$a_0^3\langle 1/r^3\rangle_{\rm NR}(p)=3.03.$$

These values correspond to a value of 130.5 MHz for $A(^1P_1)$ which, as expected, is in poor agreement with the experimental value of 58.72 MHz. The agreement is similar to that obtained by Budick and Snir.[20]

Using the values of $\langle\delta(r)/r^2\rangle_{10}(s)$ and $\langle 1/r^3\rangle_{\rm NR}(p)$, single-particle reduced matrix elements can be computed for the states of the $6s6p$ configuration. Recoupling the LS basis to jj coupling enables $A(^3P_1)$ to be expressed in terms of the contributions of $s_{1/2}$, $p_{1/2}$, and $p_{3/2}$ electrons. Furthermore, the hyperfine anomaly can now be written in terms of contributions from $s_{1/2}$ and $p_{1/2}$ electrons. For the $^3P_1$ state of Yb we find

$$\Delta=0.877\Delta(s_{1/2})+0.159\Delta(p_{1/2}),$$

which is in good agreement with the result of Unna.[23]

The same techniques can be applied to the quadrupole coupling constant, to which only the p electrons contribute. The resulting expressions can be reduced from two variables, $\langle 1/r^3\rangle_{11}(p)$ and

TABLE II. The center of gravity (c.g.) of the hyperfine components of ^{171,173}Yb and the magnetic dipole (A) and electric quadrupole (B) coupling constants for the 5556.5-Å $^3P_1$-$^1S_0$ transition.

Isotope	c.g. relative to ^{176}Yb (MHz)	A (MHz)	B (MHz)
^{171}Yb	2780.81(50)	3957.97(47)	...
^{173}Yb	1510.38(50)	−1094.20(60)	−827.15(47)

$\langle 1/r^3\rangle_{02}(p)$, to one variable using the RCF's. Using Eqs. (17) gives $\langle 1/r^3\rangle_{11}(p) = -0.045\langle 1/r^3\rangle_{02}(p)$. The resulting expressions for B, in terms of $\langle 1/r^3\rangle_{02}(p)$ are

$$B(^3P_2) = 239.84\langle 1/r^3\rangle_{02}(p),$$

$$B(^3P_2) = -134.33\langle 1/r^3\rangle_{02}(p),$$

$$B(^1P_1) = 254.27\langle 1/r^3\rangle_{02}(p),$$

where B is in MHz and $\langle 1/r^3\rangle_{02}(p)$ is in units of a_0^{-3}. The quadrupole coupling constants have been measured, in the present work, for the $^3P_1$ state and by others for the $^3P_2$ and $^1P_1$ state.[20] Each of these measurements determines a value for $\langle 1/r^3\rangle_{02}(p)$ for the corresponding P state. Values of 5.47, 6.16, and 2.38 are found for the $^3P_2$, $^3P_1$, and $^1P_1$ states. The triplet-state values are seen to be similar but the singlet-state value, as in the magnetic dipole case, is substantially different. Budick and Snir[20] obtain better agreement in the quadrupole coupling case. This is fortuitous, due to their use of an equation[22] which contains typographical errors.

In order to extract a numerical value of Δ from the experimentally determined values of A, it is necessary to correct A for second-order effects. These corrections have been computed using Eq. (21) and the energy levels and nuclear moments are listed in Table III. Also included in Table III are the corrected ratio of the dipole coupling constants and the resulting experimental value for Δ.

The only important second-order corrections are seen to be the $M1$-$M1$ corrections and they are on the order of, or smaller than, experimental errors. The dominant contribution to the $M1$-$M1$ correction is due to the nearby $^3P_0$ state.

The hyperfine anomaly parameter Δ has been extracted with an experimental error of 5%. Budick and Snir[20] have previously reported a value of $-0.376(20)$%. This value must be adjusted since they used a different,[24] now superseded,[17] value for the ratio of the nuclear magnetic moments. Budick and Snir's adjusted value for Δ is $-0.394(20)$%, in good agreement with the present value of $-0.382(19)$%, yielding an average value of $-0.388(14)$%.[25]

Using Eqs. (11)–(14) and Nilsson wave functions[8] to describe the nuclear states, a theoretical value of Δ has been calculated for Yb. The method used is similar to that of Unna[23] and the same values for the parameters σ_1, ν_2, and ν_4 were used. An effective value for g_s (the neutron-spin gyromagnetic ratio) equal to 0.7 times the free value was assumed, based upon an analysis of the magnetic moments of rare-earth nuclei.[26] The nuclear matrix elements computed using the Nilsson wave functions, were also used to compute g_k and $(g_k - g_R)b_0$. Definitions of these parameters can be found in Ref. 26. The results of the calculations and the available experimental data are listed in Table IV. It is seen that g_k, $(g_k - g_R)b_0$, and Δ are rapidly changing functions of the nuclear deformation β, but at $\beta \sim 0.3$, the Nilsson wave functions yield results for all three which are consistent with the experimental results.

TABLE IV. Magnetic moment and hyperfine anomaly parameters computed using Nilsson wave functions (Ref. 8) for the $\frac{1}{2}-$ [521] orbital for ^{171}Yb and the $\frac{5}{2}-$ [512] orbital for ^{173}Yb. The neutron spin gyromagnetic ratio g_s was renormalized by 0.7 (Ref. 26) and the experimental values for g_R and $(g_K - g_R)b_0$ were taken from Ref. 26.

	^{173}Yb	^{171}Yb		
β	g_K	g_K	$(g_K - g_R)b_0$	Δ %
0.3	−0.43	1.45	−0.44	−0.31
0.2	−0.37	0.88	−0.71	−0.62
0.1	−0.20	−0.18	−1.28	−1.54
0	−0.39	0.38	−0.56	−1.14
−0.1	−0.21	−1.58	−1.93	−1.55
−0.2	−0.01	−2.03	−2.20	−2.76
−0.3	+0.08	−2.24	−2.34	−2.90
Expt.	−0.49	1.43	−0.48	−0.388(14)

TABLE III. Second-order corrections to the magnetic dipole coupling constants and the hyperfine anomaly parameter Δ for the upper state of the 5556.5-Å transition in Yb. The atomic and nuclear data used in these calculations included: $E(^1P_1) = 25\,068.2$ cm^{-1}, $E(^3P_2) = 19\,710.4$ cm^{-1}; $E(^3P_1) = 17\,992.0$ cm^{-1}; $E(^3P_0) = 17\,288.5$ cm^{-1}; $\mu_I(171) = 0.493\,695(8)$ nm (Ref. 17); $\mu_I(173) = -0.679\,930(33)$ nm (Ref. 17); and $Q(173) = 2.8(2)$ b (Ref. 19).

	$M1$-$M1$	$M1$-$E2$	$E2$-$E2$	
$A^{(2)}(171)$ (MHz)	−0.40	...	...	
$A^{(2)}(173)$ (MHz)	−0.06	−0.0010	1.2×10^{-5}	
	Uncorrected (MHz)	Corrected (MHz)	$A(171)/A(173)$	Δ(%)
$A(171)$	3957.97(47)	3957.57(47)	−3.616 663(66)	−0.382(19)
$A(173)$	−1094.20(60)	−1094.26(60)		

V. ANALYSIS OF ISOTOPE SHIFTS

Isotope shift measurements have been the subject of several recent reviews.[27-29] A good outline of the theory and a compilation of the available experimental results have been provided by Heilig and Steudel.[27] As far as is possible, the same notation will be used here as in Ref. 27. An exception is the use of MHz, instead of mK, for the units of the isotope shifts. (1 mK $=10^{-3}$ cm^{-1} $=29.979$ MHz $=1.240\times10^{-7}$ eV.) To review briefly, the isotope shift (IS) of an atomic spectral line is the sum of a "field shift" (FS) and a "mass shift" (MS). The FS is due to a change in the spatial distribution of the nuclear charge between two isotopes. The MS is due to the difference in the nuclear kinetic energy, which is a result of the difference in the nuclear masses. The FS can be written in the factored form

$$\delta\nu_{i,\,\mathrm{field}}^{A_1A_2}=F_i\lambda^{A_1A_2}, \tag{22}$$

where A_1 and A_2 are the mass numbers of the isotopes and the subscript i labels the atomic transition. F_i is usually written as a product of an electronic factor E_i which is proportional to the change of the total nonrelativistic electron density at a point nucleus, and a computable factor $f(z)$ which includes corrections to the electron wave functions due to relativistic effects and finite nuclear size. F_i is written

$$F_i=E_if(z), \tag{23}$$

where

$$E_i=(\pi a_0^3/z)\Delta\,|\psi(0)|_i^2 \tag{24}$$

and

$$f(z)=C_{\mathrm{unif}}^{A_1A_2}\left(\frac{R_{eq}}{R_0\bar{A}^{1/3}}\right)^{2\sigma-2}\frac{1}{\delta\langle r^2\rangle_{\mathrm{unif}}^{A_1A_2}}. \tag{25}$$

In these expressions, z is the nuclear charge, a_0 is the Bohr radius,

$$\delta\langle r^2\rangle_{\mathrm{unif}}^{A_1A_2}=\tfrac{2}{5}r_0^2\bar{A}^{1/3}\delta A,$$

$$R_{eq}^2=\tfrac{5}{3}\langle r^2\rangle,$$

$$\bar{A}=\tfrac{1}{2}(A_1+A_2),$$

$$\delta A=A_2-A_1,$$

$$\sigma=(1-\alpha^2z^2)^{1/2}. \tag{26}$$

$C_{\mathrm{unif}}^{A_1A_2}$ is an isotope shift constant for a uniformly charged sphere. We use a value based on the work of Bodmer[30]:

$$C_{\mathrm{unif}}^{A_1A_2}(z)=2R_\infty\frac{1}{[\Gamma(2\sigma)]^2}\frac{1-\frac{2}{5}(1+\sigma)(1+0.01054\sigma)}{1-\frac{2}{5}(1-\sigma)(1+0.01054\sigma)}$$

$$\times\frac{2\sigma z\bar{A}}{a_0}\,\frac{2\sigma\delta A}{3\bar{A}} \tag{27}$$

where R_∞ is the Rydberg constant.

The factor $\lambda^{A_1A_2}$ contains the dependence of the IS on changes in the nuclear charge distribution between isotopes A_1 and A_2. Seltzer[31] has shown that λ can be written

$$\lambda^{A_1A_2}=\delta\langle r^2\rangle^{A_1A_2}+(C_2/C_1)\delta\langle r^4\rangle^{A_1A_2}+\cdots. \tag{28}$$

Seltzer has computed the constants C_n for K-shell electrons and points out that their ratios are also valid for optical transitions. This implies that x-ray IS and optical IS are sensitive to the same nuclear moment. Seltzer's results show that $(C_2/C_1)\sim10^{-3}$ for the rare earths so that $\lambda^{A_1A_2}\simeq\delta\langle r^2\rangle^{A_1A_2}$. It is the parameters $\lambda^{A_1A_2}$ that are extracted from an analysis of the measured optical isotope shifts.

The MS is a sum of two parts and can be written

$$\delta\nu_{i,\,\mathrm{mass}}^{A_1A_2}=\left(\frac{A_2-A_1}{A_1A_2}\right)(M_{i,\,\mathrm{normal}}+M_{i,\,\mathrm{specific}}). \tag{29}$$

The normal mass shift (NMS) is the familiar reduced mass correction and is often eliminated, from the measured IS, using $M_{i,\,\mathrm{normal}}=\nu_i/1836.1$.[27] The specific mass shift (SMS) is due to $(\vec{p}_i\vec{p}_j)$ terms in the recoil kinetic energy of the nucleus and is not readily calculated. The determination of the SMS is a major obstacle in the extraction of $\lambda^{A_1A_2}$ from measurements of optical IS.

The total IS can be written

$$\delta\nu_i^{A_1A_2}=F_i\lambda^{A_1A_2}+\left(\frac{A_2-A_1}{A_1A_2}\right)M_i. \tag{30}$$

If IS measurements are available for more than one transition it is possible to obtain a functional relationship between the measurements:

$$\left[\left(\frac{A_1A_2}{A_2-A_1}\right)\delta\nu_i^{A_1A_2}\right]=\left(\frac{F_i}{F_j}\right)\left[\left(\frac{A_1A_2}{A_2-A_1}\right)\delta\nu_j^{A_1A_2}\right]$$

$$+\left(M_i-M_j\frac{F_i}{F_j}\right) \tag{31}$$

so that if $\xi_i^{A_1A_2}=[A_1A_2/(A_2-A_1)]\delta\nu_i^{A_1A_2}$ is plotted against the same parameter for another transition j, a straight line should result. This is called a "King plot."[32] The slope and intercept of King-plot lines relate F_i and M_i for different transitions. When optical transitions are used to construct the plot, $F_i/F_j=E_i/E_j$.

A King plot can also be constructed using x-ray IS data. Since F_i and M_i can be calculated with some degree of certainty for x-ray transitions,[31]

such a plot can, in principle, be used to determine these parameters for optical transitions.[33] Since the x-ray and optical IS are sensitive to the same radial moment $\lambda^{A_1A_2}$, this procedure is valid, but severely limited by the accuracy of the available x-ray IS data.

Muonic atoms IS data can also be used to construct a King-plot line but it is well known that the radial parameter determined by the muonic IS differs from $\lambda^{A_1A_2}$, so that such a procedure will be valid only if certain conditions are satisfied.[34] Barrett[35] has shown that the FS of the muonic IS is given by

$$\delta E_{\mathrm{FS}}^{A_1A_2} = BZ\,\delta\langle r^k e^{-\alpha r}\rangle^{A_1A_2} , \tag{32}$$

where the notation is as used by Engfer *et al.*[38] In order for the King plot to yield a straight line, $\lambda^{A_1A_2}/\delta\langle r^k e^{-\alpha r}\rangle$ must be constant.

If, for example, we consider a nuclear charge distribution given by a Fermi function

$$\rho(\vec{r}) = \rho_0\left[1+\exp\left(\frac{4\ln 3(r-c)}{t}\right)\right]^{-1} \tag{33}$$

then such a ratio will be constant if $\delta c^{A_1A_2}$ and $\delta t^{A_1A_2}$ are small and proportional to each other. A frequently considered special case, which satisfies this criterion, is $\delta t^{A_1A_2}=0$. Any comparison of muonic x-ray IS data and optical IS or electronic x-ray IS data must include some model-dependent assumptions.

The isotope shift data are tabulated in Table V. The isotope shift, including the correction for the normal mass shift, has been multiplied by a mass factor to generate appropriate values for the King plot. A mass factor of $[A_1A_2/(A_2-A_1)](2/174/176)$ was used; this is close to unity, so that the listed values of $\xi_i^{A_1A_2}$ are close to the measured values of the isotope shifts. Since only one transition is measured in Yb, the usual method of plotting one optical transition against other optical transitions, cannot be applied. Instead, the published electronic and muonic x-ray IS data[36,37] are used to construct the King plot, which is shown in Fig. 4. Table V includes a tabulation of the x-ray and muonic atom data used. The quoted x-ray and muonic atom IS include all the necessary corrections to yield pure field shifts. The data points of Fig. 4 lie on a straight line reasonably well, but suggest that the x-ray and muonic data are more consistent with each other than they are with the optical IS. The reason for this is not known and may be coincidence. The x-ray and muonic IS data are significantly less accurate than the present optical IS data and this is reflected in the error bars in Fig. 4, where the uncertainties in the optical IS, which would be represented by horizontal error bars, are smaller than the plotted points.

If the x-ray and muonic atoms IS data of Fig. 4 are individually fit to straight lines, they yield

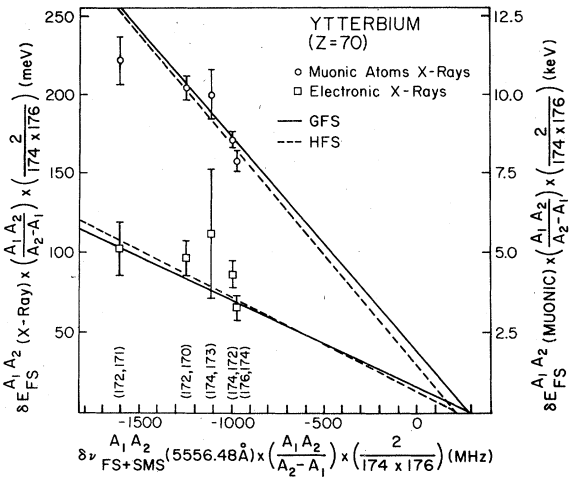

FIG. 4. King plot, for Yb, of optical shifts (5556.6 Å) vs electronic and muonic x-ray shifts. The GFS and hfs lines correspond to simultaneous fits to the muonic and electronic data using $R=1.44$ and F_i computed using the Goudsmit, Fermi, Segre method (GFS) or derived from the present analysis of hyperfine splitting (hfs), as described in the text.

TABLE V. Optical, x-ray, and muonic isotope shift data used to plot Fig. 5. Column 3 is obtained from column 2 by correcting for the normal mass shift, calculated using Eq. (29) with $M_{i,\mathrm{normal}}=\delta\nu_i/1836$. In the cases of odd isotopes, the center of gravity of the hyperfine levels was used.

		Optical isotope shift Present work (MHz)			X-ray isotope shifts from Ref. 1 (meV)		Muonic isotope shifts from Ref. 37 (keV)	
A_1	A_2	$\delta\nu_{\mathrm{obs}}^{A_1A_2}$	$\delta\nu_{\mathrm{FS+SMS}}^{A_1A_2}$	$\xi_{\mathrm{FS+SMS}}^{A_1A_2}$	$\delta E_{\mathrm{FS}}^{A_1A_2}$	$\xi_{\mathrm{FS}}^{A_1A_2}$	$\delta E_{\mathrm{FS}}^{A_1A_2}$	$\xi_{\mathrm{FS}}^{A_1A_2}$
174	176	−954.76(50)	−974.00	−974.00(50)	65.5 (74)	65.5 (74)	7.86(32)	7.86(32)
172	174	−1000.28(50)	−1019.96	−997.35(50)	88.0 (84)	86.0 (82)	8.75(23)	8.56(23)
170	172	−1286.47(50)	−1306.60	−1248.75(50)	101.4(116)	96.9(111)	10.63(36)	10.16(36)
168	170	−1368.63(50)	−1389.23	−1297.31(50)				
173	174	−555.72(50)	−565.39	−1112.8 (10)	56.8(206)	111.8(405)	5.07(40)	9.98(80)
171	172	−825.77(50)	−835.77	−1608.2 (10)	53.4 (86)	102.9(165)	5.78(37)	11.12(72)

much different values for the SMS and the F_i of the optical transition. In order to extract a meaningful SMS and F_i it is necessary to correlate the x-ray and muonic IS and perform a simultaneous fit to both sets of data. This can be accomplished by requiring that the fits to the muonic and x-ray data have the same horizontal intercept, since they should give the same SMS, and by also requiring that the ratio of their slopes on the King plot yield a value compatible with theory. This reduces the total number of free parameters and allows a more reliable determination of SMS and F_i.

The ratio of the slopes is given by

$$\frac{(\text{slope})_{\text{x-ray}}}{(\text{slope})_{\text{muonic}}} = \left(\frac{C_1}{BZ}\right)\frac{\lambda}{\delta\langle r^k e^{-\alpha r}\rangle} . \tag{34}$$

For Yb, C_1 is 623 meV/fm^2,[31] and BZ is 110.8 keV/fm^k,[37] giving $5.62R$ for the ratio, where, for convenience, we define R by

$$R \equiv \lambda/\delta\langle r^k e^{-\alpha r}\rangle . \tag{35}$$

In order to estimate R, we consider a nuclear charge distribution given by a Fermi function [Eq. (33)]. In the case of Yb, numerical integration gives

$$\lambda = 45.4\,\delta c/c + 4.95\,\delta t/t$$

and

$$\delta\langle r^k e^{-\alpha r}\rangle = 31.5\,\delta c/c + 2.88\,\delta t/t, \tag{36}$$

using $c = 6.37$ fm, $t = 2.3$ fm, $k = 2.340$, $\alpha = 0.136$ fm^{-1}, and $C_2/C_1 = -9.29\times10^{-4}$ fm^{-2}.[38,39] These expressions yield

$$R = 1.442\left(\frac{1 + 0.301\,\delta t/\delta c}{1 + 0.252\,\delta t/\delta c}\right) . \tag{37}$$

The assumption $\delta t = 0$ implies $R = 1.44$. An often used upper limit on δt is $\delta t/t = \delta c/c$, which increases R to 1.47. Attributing all the change in λ to skin-thickness variation gives $R = 1.72$.

One source of skin-thickness variations is changes in the intrinsic deformation. Using a charge distribution given by a deformed Fermi function

$$\rho(r,\theta) = \rho_0\left(1 + \exp\frac{4\ln 3[r(1 - \beta Y_{20}\cos\theta) - c]}{t_0}\right)^{-1} \tag{38}$$

yields a spherical average with an "effective skin thickness" given by[40]

$$t_{\text{eff}}^2 = t_0^2 + (4\ln 3)^2(3/4\pi^3)c^2\beta^2 + O(\beta^3). \tag{39}$$

Taking t_0 to be constant gives

$$\delta t_{\text{eff}}/t_{\text{eff}} \approx 3.57\,|\vec{\beta}|\,\delta\,|\beta| . \tag{40}$$

Zehnder *et al.*[37] have analyzed the muonic atom x-ray energies in terms of a nuclear charge distribution of the type given by Eq. (38) with a small additional term due to hexadecapole deformations, β_4. Their values for β_2 and the values obtained from the Coulomb excitation measurements of Wollersheim *et al.*[41] are listed in Table VI. Using $\bar{\beta} \approx 0.32$ as indicated by Table VI, and assuming $F_i \approx 11.0$ GHz/fm^2 (which we shall show later is a reasonable value), an estimate can be made of the fraction of the IS which is due to δt. In the worst case (^{174}Yb - ^{176}Yb), about 0.4 of the IS would be due to skin-thickness variations. This implies $\delta t/t \simeq -5.5\,\delta c/c$ and decreases R by about 6.5% to 1.35. This suggests that for individual isotope pairs, R can be expected to vary a few percent from the "constant t" value of 1.44. Remembering that the above estimate of $\delta t/t$ is for the largest $\delta\beta$ in the sequence; that some averaging of variations will occur using a King plot; and that diffuseness variations due to changes in deformation are often suppressed; a smaller value of $\delta t/t$ is to be expected. Consequently when estimating the accuracy of $\lambda^{A_1A_2}$ extracted from the data, the effect of variations in R due to skin-thickness variations are assumed to be limited by $\delta t/t = 2\delta c/c$.

As has been discussed in the review article of Heilig and Steudel,[27] the Goudsmit-Fermi-Segre (GFS) equation can be used to compute a value of $|\psi(0)|^2$ which in turn can be used to compute F_i [Eqs. (23) and (24)]. The GFS equation is a semi-empirical method based on the sequence of $2s_{1/2}$ states of the [closed core] $+ns$ configurations.[42] These states have been identified by Kaufman and Sugar[43] and, using their data, gives $(\pi a_0^3/z)\,|\psi(0)|^2_{6s} = 0.444$. Using a screening ratio γ, defined by Ref. 27 as

$$\gamma = \frac{|\psi(0)|^2_{\text{core}+ns^2} - |\psi(0)|^2_{\text{core}+nsnp}}{|\psi(0)|^2_{ns}} , \tag{41}$$

enables a value of E_i to be computed. The Hartree-Fock (HF) calculations of Wilson[44] and the relativistic Hartree-Fock (RHF) calculations of Coulthard,[45] both show that γ is nearly constant at

TABLE VI. Charge-deformation parameters for Yb. Reference 36 is muonic atom x-ray analysis of Zehnder *et al.* Reference 40 is the Coulomb excitation measurement of Wollersheim *et al.*

A	β_2 (Ref. 36)	β_2 (Ref. 40)
168	...	...
170	0.322(1)	...
171	0.327(1)	...
172	0.325(1)	0.326 (9)
173	0.324(1)	...
174	0.320(1)	0.322(10)
176	0.309(1)	0.301(10)

0.72 in the rare earths. Using a value for $f(z)$ calculated from Eq. (25) yields $F_i = 11.4$ GHz/fm^2.

It is also possible to determine $(\pi a_0^3/z)|\psi(0)|^2$ from the measured hyperfine splitting (HFS). The radial integral $\langle\delta(r)/r^2\rangle_{10}$ has the nonrelativistic limit:

$$\langle\delta(r)/r^2\rangle_{10} \to 4\pi a_0^3 |\psi(0)|^2 F_r(jl)(1-\delta), \tag{42}$$

where $F_r(jl)$ is the relativistic correction factor (RCF) of Kopfermann[14] and δ is the Rosenthal-Breit correction for finite nuclear size[46] as computed by Rosenberg and Stroke.[47] Using the value of $\langle\delta(r)/r^2\rangle_{10}$ obtained from an analysis of the HFS. $F_r(jl) = 1.784$ and, $\delta = 0.056$ gives $(\pi a_0^3/z)|\psi(0)|^2_{6s6p} = 0.346$. A screening ratio γ' similar to γ is required:

$$\gamma' = \frac{|\psi(0)|^2_{\text{core}+6s6p} - |\psi(0)|^2_{\text{core}+6s^2}}{|\psi(0)|^2_{6s6p}} . \tag{43}$$

The RHF calculation[45] for EuI gives $\gamma' = 0.881$. The HF calculation gives $\gamma' = 0.887$ for EuI and $\gamma' = 0.880$ for SmI. Assuming γ' is constant and equal to 0.88, gives $E_i = 0.305$. This yields $F_i = 10.9$ GHz/fm^2, a value which is 5% smaller than the GFS value.

Using fixed values for F_i and R, a simultaneous fit of the muonic and x-ray data to straight lines on the King plot, yields a value for the SMS and for χ^2 as defined by

$$\chi^2 = \sum_i \left(\frac{Y_i(\text{data}) - Y_i(\text{fit})}{\sigma_i} \right)^2$$

where σ_i is the experimental error. A contour plot of χ^2 and SMS in the (F_i, R) plane (see Fig. 5) yields a shallow minimum in χ^2 at $F_i \approx 12$ GHz/fm^2 and $R \approx 1.65$. This value of F_i is close to the GFS and hfs values but R implies that $\delta c \sim 0$ and gives a SMS ~ 600 MHz which is much larger than expected. Since the χ^2 contours show such a shallow minimum almost any combination of F_i and R plotted in Fig. 5 yields an acceptable fit to the data. However, other arguments presented here suggest F_i values between 10.4 and 11.9 GHz/fm^2, and R within limits determined by $\delta t/t = \pm 2\delta c/c$, are reasonable constraints. The corresponding area is indicated on Fig. 5. Although the SMS varies

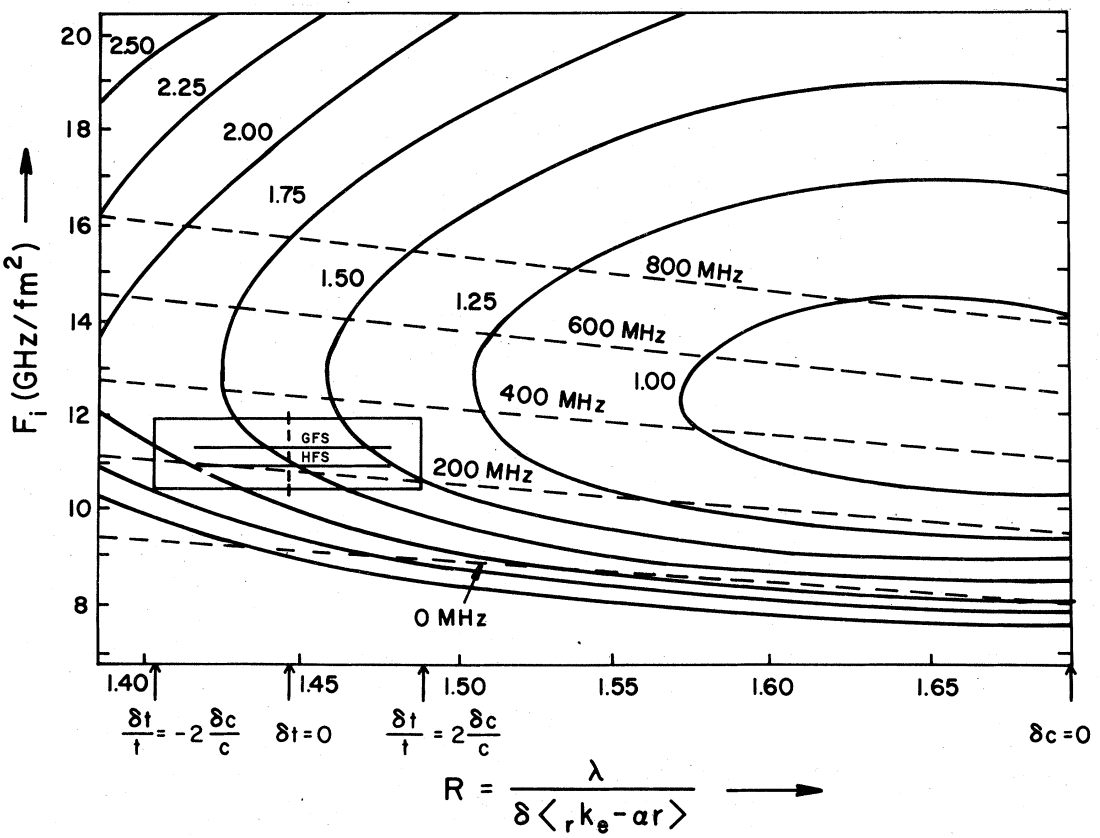

FIG. 5. Contours of χ^2 (solid lines) and SMS values (dashed lines) in the R, F_i plane. The Goudsmit-Fermi-Segre (GFS) and the hyperfine splitting (hfs) values of F_i are shown. The box indicates the variations considered in F_i and R in assigning errors to $\lambda^{A_1 A_2}$.

TABLE VII. Comparison of experimental results for $\lambda^{A_1A_2}$ and $\delta\langle r^k e^{-\alpha r}\rangle^{A_1A_2}$ for Yb isotopes. The previously reported results are from Refs. 27, 36, and 38. For the muonic atom data, $\delta\langle r^k e^{-\alpha r}\rangle$ was computed from the reported IS using $BZ = 110.8$ keV/fm^k and λ has been obtained from $\delta\langle r^k e^{-\alpha r}\rangle$ using the factor $R = 1.44$ which is computed assuming $\delta t = 0$.

		$\lambda^{A_1A_2}$ (fm^2)					$\delta\langle r^k e^{-\alpha r}\rangle$
A_1	A_2	This analysis	Optical IS	X-ray IS	X-ray+ optical	Muonic IS	Muonic IS
174	176	0.109(8)	0.087(13)	0.103(12)	0.104(11)	0.102(4)	0.071(3)
172	174	0.114(8)	0.092(15)	0.141(13)	0.138(12)	0.114(3)	0.079(2)
170	172	0.139(8)	0.116(16)	0.163(19)	0.167(16)	0.138(5)	0.096(4)
168	170	0.147(8)	0.128(19)	...	...	...	...
173	174	0.061(4)	...	0.091(33)	...	0.066(5)	0.046(4)
171	172	0.085(4)	...	0.086(14)	...	0.075(5)	0.052(4)
170	171	0.054(4)	0.041(10)	0.077(32)	0.077(32)	...	...
172	173	0.053(4)	0.041(10)	0.050(27)	0.050(27)	...	...

rapidly for changes in F_i, the values of F_i and SMS are correlated by the fit to the x-ray and muonic IS in such a way that the resulting values of $\lambda^{A_1A_2}$ are nearly constant. The rather large variation of F_i results in only ± 0.002 fm^2 variation in $\lambda^{A_1A_2}$ for $\delta A = 2$ in the worst case.

No such offsetting effect on the value of $\lambda^{A_1A_2}$ is present for variations in R. For $F_i = 11.5$ GHz/fm^2, the limits on R result in a SMS variation of ± 35 MHz. Although this is about three times smaller than the variation in SMS we consider for variations in F_i, it is not compensated by a change in F_i and results in a change in $\lambda^{A_1A_2}$ of ± 0.006 fm^2 for $\delta A = 2$.

Table VII lists values of $\lambda^{A_1A_2}$ computed using $F_i = 11.5$ GHz/fm^2 and $R = 1.44$. The assigned errors reflect the changes in $\lambda^{A_1A_2}$ that result from the uncertainties assigned to F_i and R. The results of other experimental measurements of $\lambda^{A_1A_2}$ and $\delta\langle r^k e^{-\alpha r}\rangle$ are also listed. The present values are in good agreement with the x-ray and muonic atom data, but are consistently larger than previous optical IS results.[48] The analysis leading to these latter results used nearly the same value of F_i (11.76 versus 11.5 GHz/fm^2) as used here, but used a SMS equal to half the NMS. This is a SMS of only ~10 MHz, which accounts for the consistently small values of $\lambda^{A_1A_2}$ obtained. Small values of the SMS for transitions of the type (s^2-sp), have been used throughout the literature [Ref. 27 and references therein]. This choice has been supported by the theoretical calculations of Bauche,[49] who concludes that, in the 4f series, if two configurations differ only in the number of 6s, 6p or 5d electrons, the SMS is ≤ 50 MHz.

Lines of constant SMS are included in Fig. 5 where it is seen that the value obtained is relatively insensitive to the choice of R, and hence to details of the nuclear charge distribution, but varies rapidly with F_i value. The error box drawn in the figure suggest SMS values between 150 and 350 MHz are acceptable in the present analysis. A value less than 50 MHz would imply F_i values 20% lower than the Goudsmit-Fermi-Segre value, which is difficult to justify.

The differences between our results and the x-ray and muonic atom results are not inconsistent within experimental errors. This is to be expected since we essentially normalize our results to the muonic and x-ray data. The results of the present analysis provide a more consistent set of $\lambda^{A_1A_2}$ values by normalizing the optical isotope shift precision relative measurements to the absolute, though less accurate, values from x-ray and muonic data.

The accuracy of the relative values of λ are better than the absolute values. If we define Q by

$$Q = \lambda_1/\lambda_2$$

it is easy to show that

$$\frac{\delta Q}{Q} = \frac{\delta\xi(\Delta_{\mathrm{SMS}}^2 + 2\Delta_\xi^2)^{1/2}}{(\xi_1 - \mathrm{SMS}_i)(\xi_2 - \mathrm{SMS}_i)}\ , \tag{44}$$

where Δ_{SMS} and Δ_ξ are the errors in the SMS and ξ_1 and ξ_2. $\Delta_{\mathrm{SMS}}^2 \gg \Delta\xi^2$ for our measurements. Using $\mathrm{SMS}_i = 280$ MHz and $\Delta_{\mathrm{SMS}} = \pm 100$ MHz, we find the $\delta Q/Q$ varies from 0.0015 for the ratio $\lambda^{172,174}/\lambda^{174,176}$ to 0.03 for $\lambda^{171,172}/\lambda^{174,176}$. The maximum 3% variation in the relative values of λ is a substantial improvement over about 10% variation in the value of λ.

Very few theoretical calculations of $\delta\langle r^2\rangle$ are available for deformed nuclei. The only published results for Yb isotopes[50] give 0.065 fm^2 and 0.100

fm^2 for ^{171}Yb-^{170}Yb and ^{172}Yb-^{173}Yb, respectively. The ^{171}Yb-^{170}Yb calculation is in excellent agreement with the present experimental result, but the ^{172}Yb-^{173}Yb calculation is substantially larger than obtained here.

ACKNOWLEDGMENTS

This work was supported in part by the Department of Energy under Grant No. E(11-1)-1265 and the NSF under Grant No. PHY77-21747.

*Present address: Dept. of Physics, Stanford University.
†Present address: National Bureau of Standards, Gaithersberg.
‡Present address: Dept. of Physics, Iowa State University.

[1]See, for example, *High-Resolution Laser Spectroscopy*, edited by K. Shimoda (Springer, New York, 1976).
[2]G. W. Greenlees, D. L. Clark, S. L. Kaufman, D. A. Lewis, J. F. Tonn, and J. H. Broadhurst, Opt. Commun. 23, 236 (1977).
[3]T. Kuhl, P. Dabkeiwicz, C. Duke, H. Fischer, H. J. Kluge, H. Kremmling, and E. W. Otten, Phys. Rev. Lett. 39, 180 (1977); G. Huber, C. Thibault, R. Klapisch, H. T. Duong, J. L. Vialle, J. Pinard, P. Juncar, and P. Jacquinot, Phys. Rev. Lett. 34, 1209 (1975); G. Huber, F. Touchard, S. Buttgenbach, C. Thibault, R. Klapisch, S. Liberman, J. Pinard, H. T. Duong, P. Juncar, J. L. Vialle, P. Jacquinot, and A. Pesnelle, Phys. Rev. Lett. 41, 459 (1978); G. Nowicki, K. Bekk, S. Goering, H. Hanser, H. Rebel, and G. Schatz, Phys. Rev. Lett. 39, 332 (1977), and references contained therein.
[4]J. H. Broadhurst, M. E. Cage, D. L. Clark, G. W. Greenlees, J. A. R. Griffith, and G. R. Isaak, J. Phys. B 7, L513 (1974).
[5]R. G. H. Robertson, J. C. Waddington, and R. G. Summers-Gill, Can. J. Phys. 46, 2499 (1968); W. J. Childs, Phys. Rev. A 2, 1692 (1970); K. F. Smith and P. J. Unsworth, Proc. Phys. Soc. London 86, 1249 (1965).
[6]L. Armstrong, Jr., *Theory of the Hyperfine Structure of Free Atoms* (Wiley-Interscience, New York, 1971).
[7]C. Schwartz, Phys. Rev. 97, 380 (1955).
[8]J. P. Davidson *Collective Models of the Nucleus* (Academic Press, New York, 1968), Appendix D, p. 183.
[9]D. L. Clark, Ph.D. thesis (University of Minnesota, 1977) (unpublished).
[10]H. H. Stroke, R. J. Blin-Stoyle, and V. Jaccarino, Phys. Rev. 123, 1326 (1961).
[11]A. S. Reiner, Nucl. Phys. 5, 544 (1958).
[12]S. G. Nilsson, Dan. Mat. Fys. Medd. 29, No.16 (1955).
[13]P. G. H. Sandars and J. Beck, Proc. R. Soc. London Ser. A 289, 97 (1965).
[14]H. Kopferman *Nuclear Moments* (Academic, New York, 1958), p. 445.
[15]W. J. Childs and L. S. Goodman, Phys. Rev. A 6, 1772 (1972).
[16]M. Baumann and G. Wandel, Phys. Lett. A 28, 200 (1968).
[17]L. Olschewski, Z. Phys. 249, 205 (1972).
[18]J. S. Ross and K. Murakawa, Phys. Rev. 128, 1159 (1962).
[19]J. S. Ross and K. Murakawa, J. Phys. Soc. Jpn. 19, 249 (1964).
[20]B. Budick and J. Snir, Phys. Rev. 178, 18 (1969).
[21]M. Bauman, H. Liening, and H. Lindel, Phys. Lett. A 59, 433 (1977).
[22]A. Lurio, Phys. Rev. 142, 46 (1966). We believe Eq. (6) of this paper should be modified so that the last term is written

$$\frac{\beta^2}{2l+1}\left[\left(\frac{(2l-1)(l+2)}{2l+1}+\frac{6\eta}{2l+1}\right)b^{SS}_{l+1/2}+lb^{SS}_{l-1/2}\right].$$

Also the preceeding term contains a typographical error in that the second $b^{ST}_{l+1/2}$ should be $b^{ST}_{l-1/2}$.
[23]I. Unna, Phys. Lett. B 24, 499 (1967).
[24]L. Olschewski and E. W. Otten, Z. Phys. 200, 224 (1967).
[25]The value reported earlier by our group (Ref. 4) is in error due to a computational mistake.
[26]A. Bohr and B. R. Mottelson, *Nuclear Structure* (Benjamin, New York, 1975), Vol. II, p. 302.
[27]K. Heilig and A. Steudel, At. Data Nucl. Data Tables 14, 613 (1974).
[28]R. C. Barrett, Rep. Prog. Phys. 37, 1 (1974).
[29]H. H. Stroke, J. Phys. Soc. Jpn. Suppl. 34, 543 (1973).
[30]A. R. Bodmer, Proc. Phys. Soc. London Ser. A 66, 1041 (1953).
[31]E. C. Seltzer, Phys. Rev. 188, 1916 (1969).
[32]W. H. King, J. Opt. Soc. Am. 53, 638 (1963).
[33]The usual notation for x-ray and muonic IS assigns to the parameter F_i the symbol C_i for x-ray IS and BZ muonic IS.
[34]C. S. Wu, in *International Symposium on Nuclear Structure*, Dubna 1968 (IAEA, Vienna, Austria, 1969), p. 367.
[35]R. C. Barrett, Phys. Lett. B 33, 388 (1970).
[36]P. L. Lee and F. Boehm, Phys. Rev. C 8, 819 (1973).
[37]A. Zehnder, F. Boehm, W. Dey, R. Engfer, H. K. Walter, and J. L. Vuilleumier, Nucl. Phys. A 254, 315 (1975).
[38]R. Engfer, H. Schneuwly, J. L. Vuilleumier, H. K. Walter, and A. Zender, At. Data Nucl. Data Tables 14, 509 (1974).
[39]F. Boehm and P. L. Lee, At. Data Nucl. Data Tables 14, 605 (1974).
[40]J. H. Heisenberg, J. S. McCarthy, I. Sick, and M. R. Yearian, Nucl. Phys. A 164, 340 (1971).
[41]H. J. Wollersheim, W. Wilcke, and T. W. Elze, Phys. Rev. C 11, 2008 (1975).
[42]I. I. Sobel'man, *An Introduction to the Theory of Atomic Spectra* (Pergamon, New York, 1972).
[43]V. Kaufman and J. Sugar, J. Opt. Soc. Am. 63, 1168 (1973).
[44]M. Wilson, J. Phys. B 5, 218 (1972).
[45]M. A. Coulthard, J. Phys. B 6, 23 (1973).
[46]J. E. Rosenthal and G. Breit, Phys. Rev. 41, 459 (1932).
[47]H. J. Rosenberg and H. H. Stroke, Phys. Rev. A 5, 1992 (1972).
[48]The discrepancy between previous optical IS results and the electron x-ray data has been noted by Gerstenkorn, J. Phys. Suppl. (Paris) 34, 55 (1973).
[49]J. Bauche, J. Phys. 35, 19 (1974).
[50]D. Zawischa and J. Speth, Phys. Lett. B 56, 225 (1975).